Local structural phenomena in pure and Ru-doped $0.9PbZn_{1/3}Nb_{2/3}O_3 - 0.1PbTiO_3$ near the morphotropic phase boundary as revealed by Raman spectroscopy

N. Waeselmann,[1,*] B. Mihailova,[1,*] B. J. Maier,[1] C. Paulmann,[1] M. Gospodinov,[2] V. Marinova,[3] and U. Bismayer[1]

[1]*Department Geowissenschaften, Universität Hamburg, Grindelallee 48, D-20146 Hamburg, Germany*
[2]*Institute of Solid State Physics, Bulgarian Academy of Sciences, Boulevard Tzarigradsko Chausse 72, BG-1784 Sofia, Bulgaria*
[3]*Institute of Optical Materials and Technologies, Bulgarian Academy of Sciences, Acad. G. Bonchev Str. 109, BG-1113 Sofia, Bulgaria*

The development of polar order in perovskite-type (ABO_3) solid solutions of relaxors and normal ferroelectrics is studied on the basis of the temperature dependence of polarized Raman spectra of pure and Ru-doped $0.9PbZn_{1/3}Nb_{2/3}O_3$-$0.1PbTiO_3$ (PZN-0.1PT) single crystals as well as complementary x-ray diffraction analysis. It is shown that the Raman peaks related to Pb-localized vibrations existing solely in a double-perovskite structure (prototype symmetry $Fm\bar{3}m$) are highly sensitive to the nucleation and development of polar atomic arrangements. The doublet near 50 cm^{-1} observed in the high-temperature $\bar{Z}(XY)Z$ spectra of PZN-xPT ($x = $ 0–0.1) is attributed to two distinct cubic states of Pb ions in regions with a local chemical B-site order of the type $Pb(B_{2/3}^{2+}B_{1/3}^{5+})_{0.5}B_{0.5}^{5+}O_3$: Pb1 ions surrounded mainly by Nb^{5+} and Pb2 ions surrounded by both Zn^{2+} and Nb^{5+}. The singlet in the high-temperature $\bar{Z}(XY)Z$ spectra is assigned to off-centered Pb2 ions. The Raman spectra of PZN-0.1PT indicate that off-centered Pb2 ions induce coherent polar shifts of ferroelectrically active B cations, which in turn facilitates the off-centering of Pb1 ions. A low degree of B-site doping with mixed-valence elements like Ru can substantially influence the development of ferroelectric order in PZN-xPT solid solutions due to the different preferred types of local octahedral distortion associated with the different valence states of the doping cations. The incorporation of Ru into the structure of PZN-0.1PT slightly decreases the Burns temperature and shifts the tetragonal-to-monoclinic phase transition to lower temperatures, thus favoring the tetragonal state in a wider temperature range as compared to the undoped compound. An assumption is made that the nanoscale polar order in Pb-based B-site complex perovskite-type relaxors might be of *ferrielectric type* rather than of ferroelectric type.

I. INTRODUCTION

Perovskite-type (ABO_3) solid solutions $(1–x)PbZn_{1/3}Nb_{2/3}O_3$-$xPbTiO_3$ (PZN-xPT) have been extensively studied during the past decade because of their excellent piezoelectric and dielectric properties essential for various technological applications.[1] The individual components of PZN-xPT are quite different in their structural behavior, leading to a very complex local structure of the mixed compound. $PbTiO_3$ (PT) is a normal ferroelectric undergoing a cubic-to-tetragonal phase transition at the Curie temperature T_C, while $PbZn_{1/3}Nb_{2/3}O_3$ (PZN) is a relaxor ferroelectric (or relaxor) undergoing a sequence of phase transformations from a cubic to a rhombohedral phase with a few intermediate states consisting of polar nanoregions dispersed into a nonpolar matrix.[2,3] Polar nanoclusters with reorientation dynamics nucleate at the so-called Burns temperature T_B (well above T_C), and at the characteristic temperature T^* (between T_B and T_C) they couple to form larger polar nanoregions with slower flipping dynamics.[4,5] In addition, PZN possesses a strong chemical inhomogeneity due to the occupation of the B site by two- and five-valent cations. This leads to a frustration between charge neutrality and lattice strain, which on the local scale results in the formation of chemically 1:1 B-site ordered nanoregions of type $A(B_{2/3}^{2+}B_{1/3}^{5+})_{0.5}B_{0.5}^{5+}O_3$.[6] The alternating chemical ordering of the B cations along the cubic ⟨100⟩ directions leads to a doubling of the unit cell and hence, in a paraelectric state the symmetry of the chemically ordered and disordered regions is $Fm\bar{3}m$ and $Pm\bar{3}m$, respectively. The

piezoelectric and dielectric responses of PZN-xPT are largest close to the morphotropic phase boundary (MPB),[7,8] which corresponds to $x \sim$ 0.08–0.10.[9] In the ferroelectric state, compositions with $x < 0.08$ show rhombohedral symmetry whereas those with $x > 0.10$ have tetragonal symmetry. The structural state at the MPB is still controversial. Based on synchrotron x-ray diffraction (XRD) analysis on poled samples it has been proposed that the polarization path between the rhombohedral and tetragonal phases is realized via an intermediate monoclinic phase,[10] similar to other ferroelectric solid solutions.[11,12] Further XRD studies on poled PZN-xPT single crystals revealed the existence of an orthorhombic phase in a narrow x range with near-vertical boundaries on both sides.[9] The orthorhombic phase has the space group $Amm2$ with the net polarization **P** being along the cubic [011] direction, which is the limiting case of the monoclinic phase Pm, also called the M_C phase,[12] with **P** along the cubic [0υw] direction. Neutron diffraction on unpoled crystals showed that at the MPB an orthorhombic or monoclinic phase may exist along with a tetragonal phase.[13] On the other hand, piezoresponse force microscopy studies give evidence for the coexistence of domains with various symmetries, including a possible combination of rhombohedral and tetragonal symmetries.[14,15] The structure of PZN-xPT is even more puzzling because above the critical temperature polar nanoregions (PNRs) are formed (as in the case of relaxors) and at $T < T_C$ the PNRs persist, coexisting with the complex pattern of ferroelectric domains with established long-range order.[16] Neutron elastic

diffuse scattering revealed that the internal structure of PNRs is independent of x and is most probably rhombohedral type, but the growth direction of PNRs changes from the cubic $\langle 111 \rangle$ to approximately $\langle 001 \rangle$ direction when x increases from 0 to 0.09.[17] Recently, it has been suggested that the coupling between PNRs and acoustic phonons may be the key factor for the remarkable electromechanical properties of PZN-xPT and of the similar system $(1-x)$PbMg$_{1/3}$Nb$_{2/3}$O$_3$-xPbTiO$_3$ (PMN-xPT) rather than the coexistence and competition of domains with different types of ferroelectric long-range order.[18] This underlines the importance of studying the development of mesoscopic or intermediate-range order in relaxor-based solid solutions. Raman spectroscopy,[19] acoustic emission,[20] and Brillouin spectroscopy[21] clearly revealed that PZN-xPT exhibit both T_B and T^*, which are characteristic temperatures for relaxors. For PZN-xPT at the MPB ($x = 0.09$) $T_B \sim 730$ K, $T^* \sim 525$ K, and upon further cooling two phase transitions occur: a cubic-to-tetragonal (C-T) at $T_{C1} \sim 450$ K and a tetragonal-to-M$_C$ type (T-M) at $T_{C2} = 340$ K.[20] Both phase transitions show a thermal hysteresis, as $T_{C1}^{\text{heating}} - T_{C1}^{\text{cooling}} \sim 10$ K and $T_{C2}^{\text{heating}} - T_{C2}^{\text{cooling}} \sim 40$ K for the C-T and T-M transitions, respectively.[20]

Raman spectroscopy has been proved to be an excellent tool for studying the fine-scale transformation processes in relaxors on the basis of the temperature evolution of phonon anomalies.[4,5,22] Renormalization phenomena due to the addition of PbTiO$_3$ have been demonstrated by a thorough Raman scattering analysis on PZN-xPT for $x = 0.045$, which is, however, on the rhombohedral side of the phase diagram. Raman spectroscopic studies have been conducted also for PZN-xPT systems for $x = 0.08$ (Refs. [23,24]) and $x = 0.09$ (Ref. [25]), which are at the MPB, but the analysis was focused mainly on the structure of the long-range ordered ferroelectric phases. The objective of this paper was to apply polarized Raman spectroscopy in the temperature range 100–850 K as well as complementary XRD to study the development of polar atomic arrangements in PZN-0.1PT, which is exactly on the right-hand-side border of the narrow MPB. The structural analysis is performed also on Ru-doped PZN-0.1PT, as recently it has been demonstrated that a low degree of Ru doping leads to considerable hardening of the polarization- and strain-electric field loops.[15]

II. EXPERIMENTAL DETAILS

Optically and chemically homogeneous single crystals of PZN-0.1PT and PZN-0.1PT : Ru with the ratio Ru/Ti ~ 0.02 were synthesized by the high-temperature solution growth method.[15] The chemical composition of the as-grown single crystals was determined by electron microprobe analysis (Cameca Microbeam SX100) averaging over 50 points from each specimen. The relative error in the x value was 0.3% as determined from the standard deviation of the Ti content, whereas the standard deviation of the Ru content was $\sim 35\%$.

Powder XRD measurements were performed with a Philips X'Pert diffractometer (Bragg-Brentano geometry), using an Anton Paar high-temperature cell. The experiments were conducted on heating in the range 300–850 K. The XRD patterns were collected with Cu Kα radiation in a 2θ range from 20° to 80°, with a step size of 0.02° and an accumulation time of 10 s per step. Synchrotron single-crystal XRD was performed at the F1 beamline at HASYLAB/DESY using a MarCCD 165 detector. Data were collected with a radiation wavelength of $\lambda = 0.4000$ Å, a sample-to-detector distance of 100 mm, a step width of 0.5° per frame, and an exposure time of 220 s. For both PZN-0.1PT and PZN-0.1PT : Ru experiments were carried out at $T = 300$ and 150 K with an open-flow liquid-N$_2$ cryostat (Oxford Cryosystems, Series 600). Reciprocal lattice sections were reconstructed using the in-house developed software RASTM.[26]

Raman spectra were collected using a Horiba Jobin-Yvon T64000 triple-grating spectrometer equipped with an Olympus BH41 microscope and a 50× long-working distance objective. The measurements were conducted in backscattering geometry using the 514.5-nm line of an Ar$^+$ laser and a spectral resolution of 2 cm^{-1}. Pure PZN-xPT was measured with a power density on the sample surface of 2.8 kW/mm^2, an acquisition time of 15 s, and averaging over 10 loops. The corresponding experimental conditions for the Ru-doped sample were 1.4 kW/mm^2, 30 s, and 10 loops; a lower laser power had to be used for the Ru-doped compound in order to avoid sample overheating under laser irradiation due to the difference in the optical properties. The *in situ* temperature-dependent experiments were conducted in a Linkam heating-coolingstage ensuring a temperature stability of ± 0.1 K. Polarized spectra were collected upon cooling from 850 to 100 K with a relatively small temperature step in $\bar{Z}(XX)Z$ and $\bar{Z}(XY)Z$ scattering geometries (Porto's notation), where X, Y, and Z are parallel to the cubic [100], [010], and [001] crystallographic directions, respectively. For selected temperatures $\bar{Z}(X'X')Z$ and $\bar{Z}(X'Y')Z$ spectra were additionally measured, where X' and Y' denote the cubic [110] and [$\bar{1}$10] crystallographic directions, respectively. The as-measured spectra were reduced by $n(\omega, T) + 1$, where $n(\omega, T) = 1/(e^{\hbar\omega/kT} - 1)$ is the Bose-Einstein phonon distribution, to eliminate the effect of temperature on the peak intensities and fitted with Lorentzian functions to determine the peak positions, full widths at half maximum (FWHMs) and intensities, using the software package ORIGIN 8.1. All peak parameters, namely, the peak positions, FWHMs, and integrated intensities were variables during the fitting procedure.

III. RESULTS AND DISCUSSION

A. XRD analysis

We have applied powder XRD analysis to detect the phase transitions occurring at elevated temperatures. Figure 1 displays the powder XRD patterns of pure and Ru-doped PZN-0.1PT in the 2θ range that corresponds to the 100 Bragg peak indexed in $Pm\bar{3}m$ (or 200 Bragg peak in $Fm\bar{3}m$). The C-T phase transition takes place between 475 and 450 K as revealed by the existence of an additional shoulder near $2\theta = 21.8°$, due to the splitting of the cubic Bragg peak below T_{C1}. The diffraction peak profile is somehow changed below 375 K, where the T-M phase transition is expected to occur, but the strong signal overlapping and insufficient resolution of in-house diffraction experiments hindered the precise phase determination. At 300 K the diffraction peak seems to consist
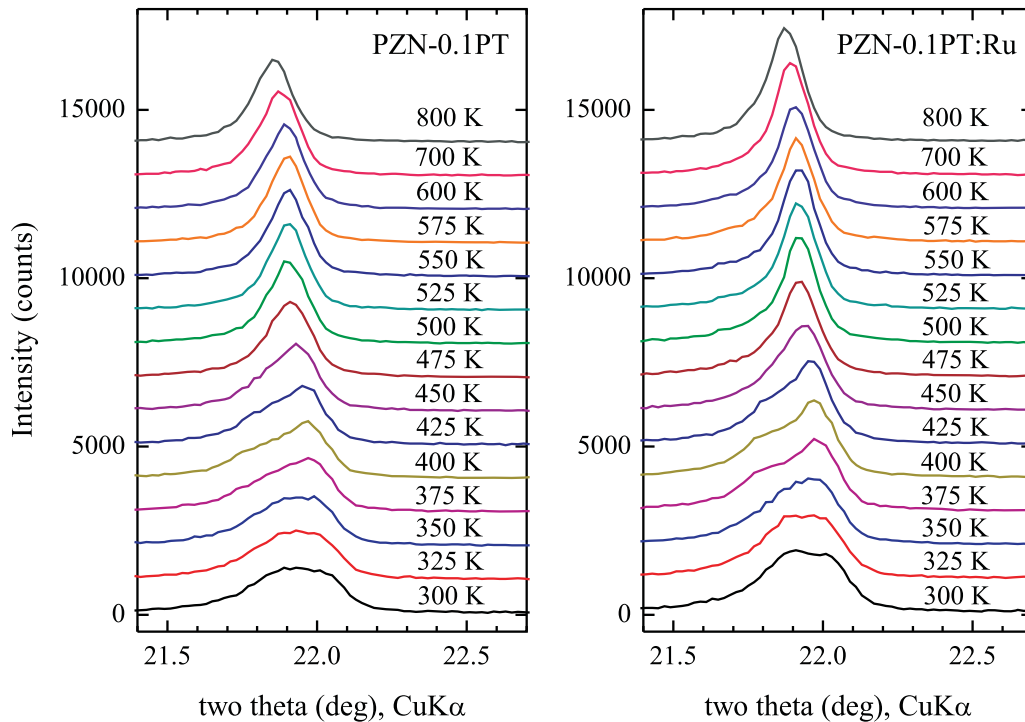
FIG. 1. (Color online) Powder XRD patterns of pure and Ru-doped PZN-0.1PT; the 2θ range corresponds to the 100 Bragg peak indexed in $Pm\bar{3}m$, which is equivalent to the 200 Bragg peak in $Fm\bar{3}m$.

of more than two components, indicating the coexistence of a phase (or phases) with symmetry different from tetragonal. This is in accordance with piezoresponse force microscopy experiments demonstrating the coexistence of at least two types of domains at room temperature[15] and confirms that the compounds studied here are at the MPB.

The existence of PNRs possessing a ferroelectric order on the intermediate scale is unique for relaxors and relaxor-based systems. Since PNRs are local ferroic inhomogeneities in the average structure, the observation of x-ray diffuse scattering is a direct indicator of their presence.[27,28] To check if in both pure and Ru-doped PZN-0.1PT PNRs persist at low temperatures, we have conducted synchrotron single-crystal XRD at $T =$ 300 and 150 K, i.e., below T_{C2}. The $(hk0)$ and $(hk1)$ layers (indexation given in $Fm\bar{3}m$) of the reciprocal space reconstructed from synchrotron single-crystal XRD data collected on PZN-0.1PT and PZN-0.1PT : Ru are presented in Fig. 2. X-ray diffuse scattering streaks along the $\langle110\rangle^*$directions are clearly visible in the $(hk0)$ layers, revealing the existence of PNRs well below the T-M phase transition temperature. These streaks originate from off-center cation displacements which correlate within {110} planes of the real space and are typical of Pb-based relaxors.[27,28] The weak diffuse spots in the $(hk1)$ layers are also due to PNRs. Monte Carlo simulations show that the observed $\langle110\rangle^*$ diffuse scattering can be reproduced fairly well using Pb displacements along each of the cubic $\langle111\rangle$, $\langle110\rangle$, and $\langle100\rangle$ directions,[27,28] but detailed experimental studies of the neutron diffuse scattering around the 110 reciprocal lattice point suggest the PNRs in PZN-xPT have an inherent rhombohedral distortion.[2,17] The fraction of PNRs seems to be slightly larger in the Ru-doped compound than that in the undoped compound as evident by

the slightly stronger x-ray diffuse scattering intensity. For both pure and Ru-doped PZN-0.1PT the x-ray diffuse scattering intensity increases when temperature decreases from 300 to 150 K, indicating that the PNRs further develop in a competing coexistence with the long-range polar order of M_C type.

The absence of any sharp Bragg peaks with h, k, $l =$ all odd (see the $hk1$ layers in Fig. 2) indicates that there is no long-range chemical B-site 1:1 order that would lead to a doubling of the unit cell within spatial regions large enough to be detected by synchrotron single-crystal XRD.

B. Raman scattering of PZN-0.1PT

Polarized Raman spectra of PZN-0.1PT collected at different temperatures in $\bar{Z}(XX)Z$ and $\bar{Z}(XY)Z$ geometries are shown in Fig. 3. On the length scale of sensitivity of Raman scattering, Pb-based relaxors exhibit a double-perovskite structure, as clearly revealed by the existence of peaks near 800 and 50 cm^{-1}.[4,29–32] These peaks originate from first-order Raman scattering related to cubic Raman-active nondegenerate and triply degenerate modes of the prototype structure, respectively, which are symmetry allowed only in a double-perovksite structure.[4,29–32] In a single-perovskite structure such modes do not exist, no matter if the structure is cubic or ferroically distorted. A moderate addition of PT to PZN or PMN does not disturb the doubling of the perovskite structure.[19,23,24] Four phonon modes are Raman active in the prototype cubic double-perovskite structure ($Fm\bar{3}m$): A_{1g} + E_g + $2F_{2g}$.[33] The A_{1g} and E_g modes are active in $\bar{Z}(XX)Z$ geometry while the two F_{2g} modes are active in $\bar{Z}(XY)Z$ geometry. As can be seen in Fig. 3, more peaks than symmetry allowed are observed above T_{C1} due to the presence of ferroic
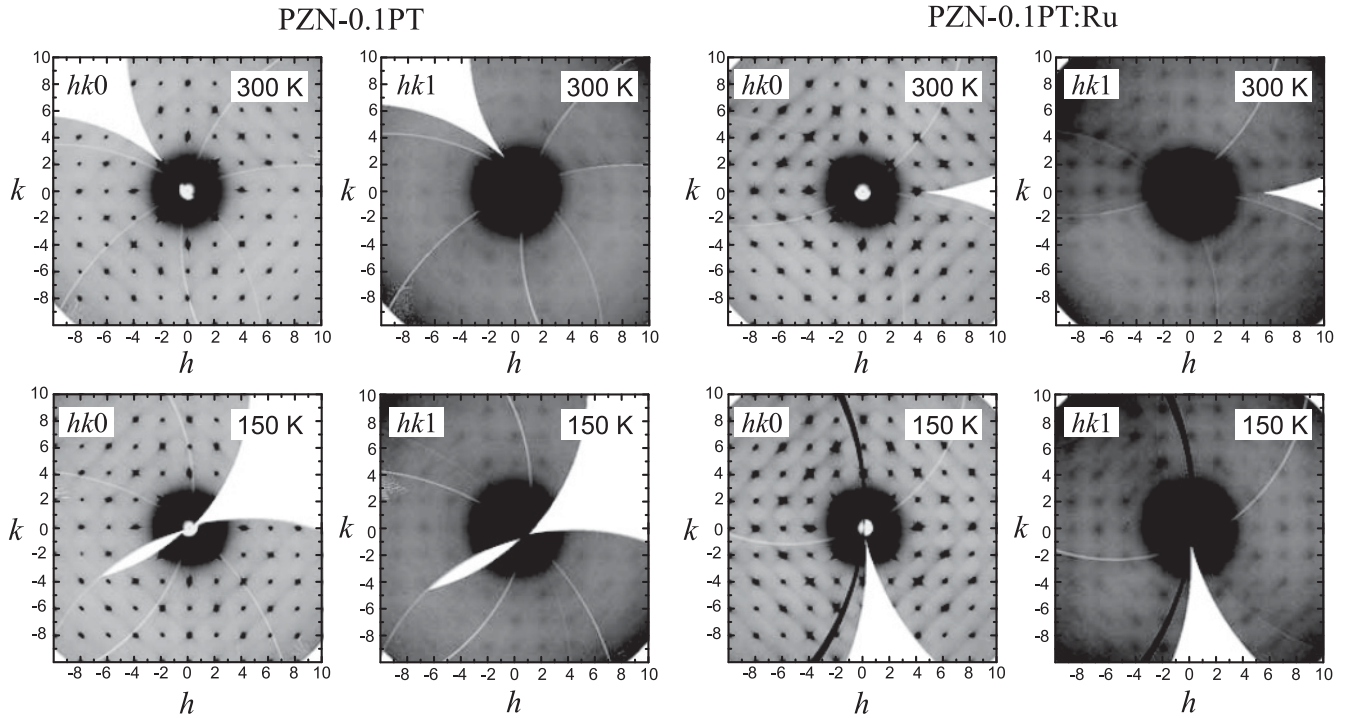
PZN-0.1PT

PZN-0.1PT:Ru

FIG. 2. Reciprocal-lattice layers reconstructed from synchrotron single-crystal XRD on pure and Ru-doped PZN-0.1PT. The Miller indices refer to a cubic double-perovskite $Fm\bar{3}m$ unit cell.

atomic arrangements with a lifetime longer than the time-scale sensitivity of Raman spectroscopy determined by the phonon time period, which is of order 10^{-12}–10^{-13} s. It has been previously demonstrated that the Raman scattering near 50 and 260 cm^{-1} is very sensitive to structural transformations in Pb-based relaxors[5,31,34] and thus, we analyzed in more detail
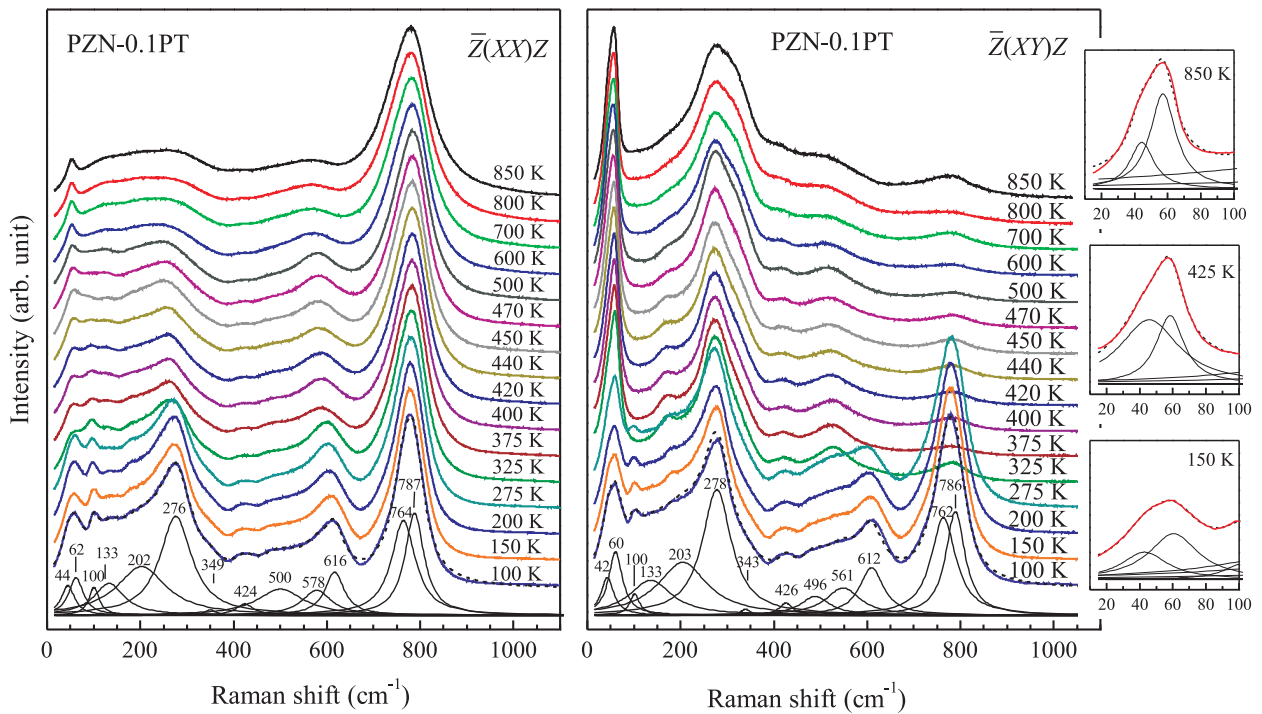

FIG. 3. (Color online) Parallel- $\bar{Z}(XX)Z$ and cross- $\bar{Z}(XY)Z$ polarized Raman scattering of PZN-0.1PT collected at different temperatures in the range 100–850 K; thin lines represent the fitting Lorentzians used for 100 K. Insets on right show on an enlarged scale the band near 50 cm^{-1} measured in $\bar{Z}(XY)Z$ geometry (red bold curves), the corresponding fitting Lorentzians (thin curves), and resultant spectrum profiles (black dashed curves).

the temperature dependence of the corresponding peaks in the Raman spectra of PZN-01.PT.

1. Assignment of the doublet observed at high temperatures in $\bar{Z}(XY)Z$ geometry

The band near 50 cm^{-1} arises from the Pb-localized F_{2g} mode and at $T > T_{C1}$ one peak should be observed in the $\bar{Z}(XY)Z$ spectrum. However, even at 850 K two peaks are well resolved in the $\bar{Z}(XY)Z$ spectrum of PZN-0.1PT (see Fig. 3). For relaxors of the type $PbB'_{0.5}B''_{0.5}O_3$ and $Pb(B'_{0.5}B''_{0.5})_{1-x}B'''_x O_3Pb$, one strong peak coming from the cubic F_{2g} mode is observed at high temperatures in $\bar{Z}(XY)Z$ geometry, in accordance with the group-theory analysis; a corresponding weak "forbidden" peak is observed in $\bar{Z}(XX)Z$ geometry, due to the presence of Pb off-centered displacements.[5,31,34] Therefore, if the second peak in the $\bar{Z}(XY)Z$ spectrum of PZN-0.1PT is caused by additional ferroic distortions, a corresponding component should exist in the $\bar{Z}(XX)Z$ spectrum. However, at high temperatures there is only one "forbidden" $\bar{Z}(XX)Z$ peak instead of two, suggesting that the two peaks in the $\bar{Z}(XY)Z$ spectra of PZN-0.1PT are related to two different cubic vibrational states of Pb atoms. This assumption is strongly supported by the fact that when the polarization of the incident light is along the cubic face diagonal, both peaks near 50 cm^{-1} are suppressed in the cross-polarized $\bar{Z}(X'Y')Z$ spectrum and enhanced in the parallel-polarized $\bar{Z}(X'X')Z$ spectrum (see Fig. 4), following the transformation rules of the Raman polarizability tensor for cubic F_{2g} modes.[29] Two peaks near 50 cm^{-1} in the $\bar{Z}(XY)Z$ spectra and only one peak near 50 cm^{-1} in the $\bar{Z}(XX)Z$ spectra are also observed for PMN, PZN, and PZN-xPT for $x = 0.045$ and 0.08, but not for $x = 0.20$.[19,23,30,35] These findings indicate that the discussed vibrational states of Pb are not due to possible chemical separation of PZN-rich and PT-rich regions, but they are exclusively typical of $PbB'_{1/3}B''_{2/3}O_3$ systems. On the local scale, $PbB'_{1/3}B''_{2/3}O_3$ compounds also exhibit chemically 1:1 B-site ordered regions as in the case of $PbB'_{0.5}B''_{0.5}O_3$ compounds, but due to the different stoichiometry, the ordered regions are of the type $Pb(B^{2+}_{2/3}B^{5+}_{1/3})_{0.5}B^{5+}_{0.5}O_3$.[6] Therefore, in $PbB'_{1/3}B''_{2/3}O_3$ systems with a doubled unit cell, there is a high probability to have Pb ions surrounded entirely by the higher-valence B'' cations (see the sketch in Fig. 5) as well as by both B' and B'' cations, as in the case of $PbB'_{0.5}B''_{0.5}O_3$ systems. Hence, there are two cubic vibrational states of Pb ions: Pb1, surrounded only by B^{5+}, and Pb2, surrounded by both B^{2+} and B^{5+}. The former state is more constrained because Pb^{2+} experiences strong repulsive interactions from all surrounding B cations, which should oppose the intrinsic affinity of Pb^{2+} to form a lone pair and hence to displace off the center of the cubo-octahedral cavity. By contrast, the second state allows for more flexibility and Pb2 ions may easily displace away from the octahedral center, for example, along $\langle 110 \rangle$ to compensate the underbonded oxygen ions[36] shared between B^{2+} and B^{5+} cations in locally ordered regions of $PbB'_{1/3}B''_{2/3}O_3$ systems or along $\langle 111 \rangle$ between two B cations with different valence.[37] The latter structural distortion can be realized also in $PbB'_{0.5}B''_{0.5}O_3$ systems and is in agreement with the proposed rhombohedral-type structure of PNRs.[2,17]
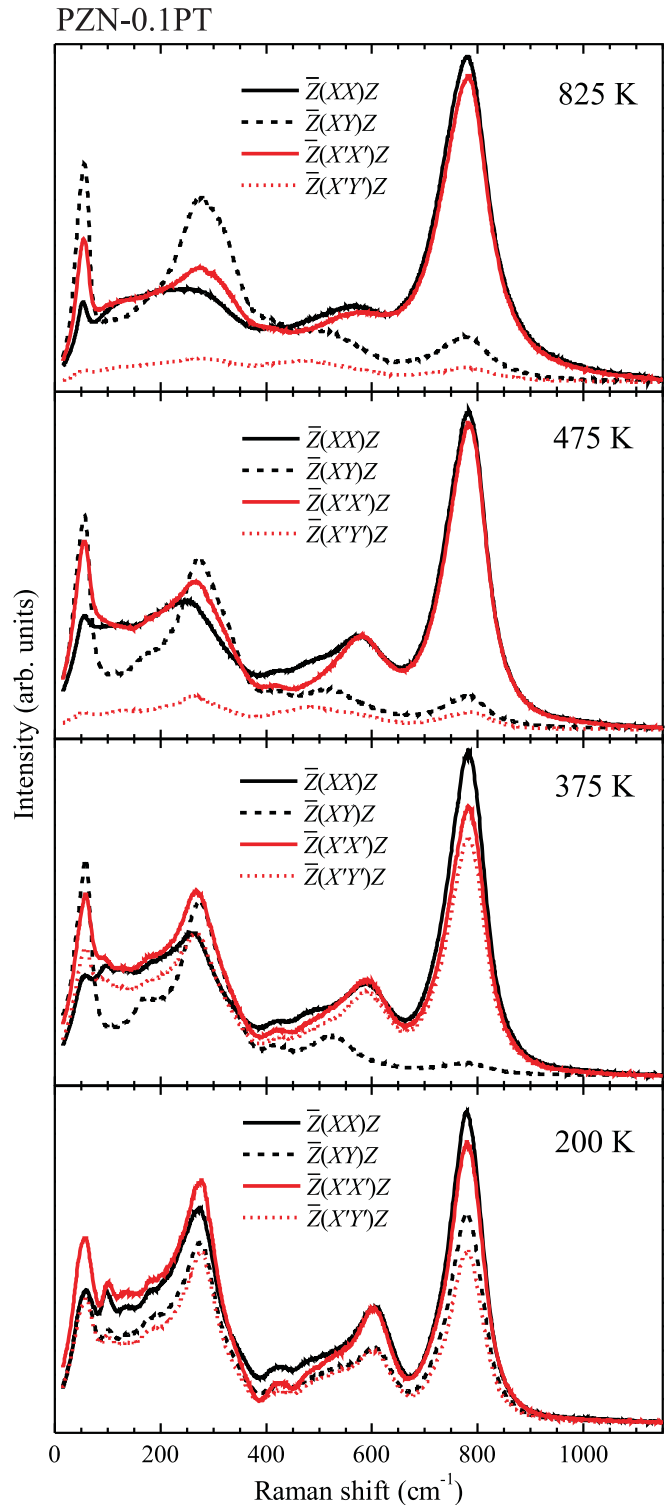

FIG. 4. (Color online) Parallel- and cross-polarized Raman spectra of PZN-0.1PT collected at selected temperatures with the incident light polarization parallel to the cubic edge [$\bar{Z}(XX)Z$ and $\bar{Z}(XY)Z$] and parallel to the cubic face diagonal [$\bar{Z}(X'X')Z$ and $\bar{Z}(X'Y')Z$].

As a result, at high temperatures the vibrations of Pb1 ions should contribute to one peak in the $\bar{Z}(XY)Z$ spectrum and to none in the $\bar{Z}(XX)Z$ spectrum; Pb2 ions should contribute to one peak in the $\bar{Z}(XY)Z$ spectrum and a part of Pb2 ions,
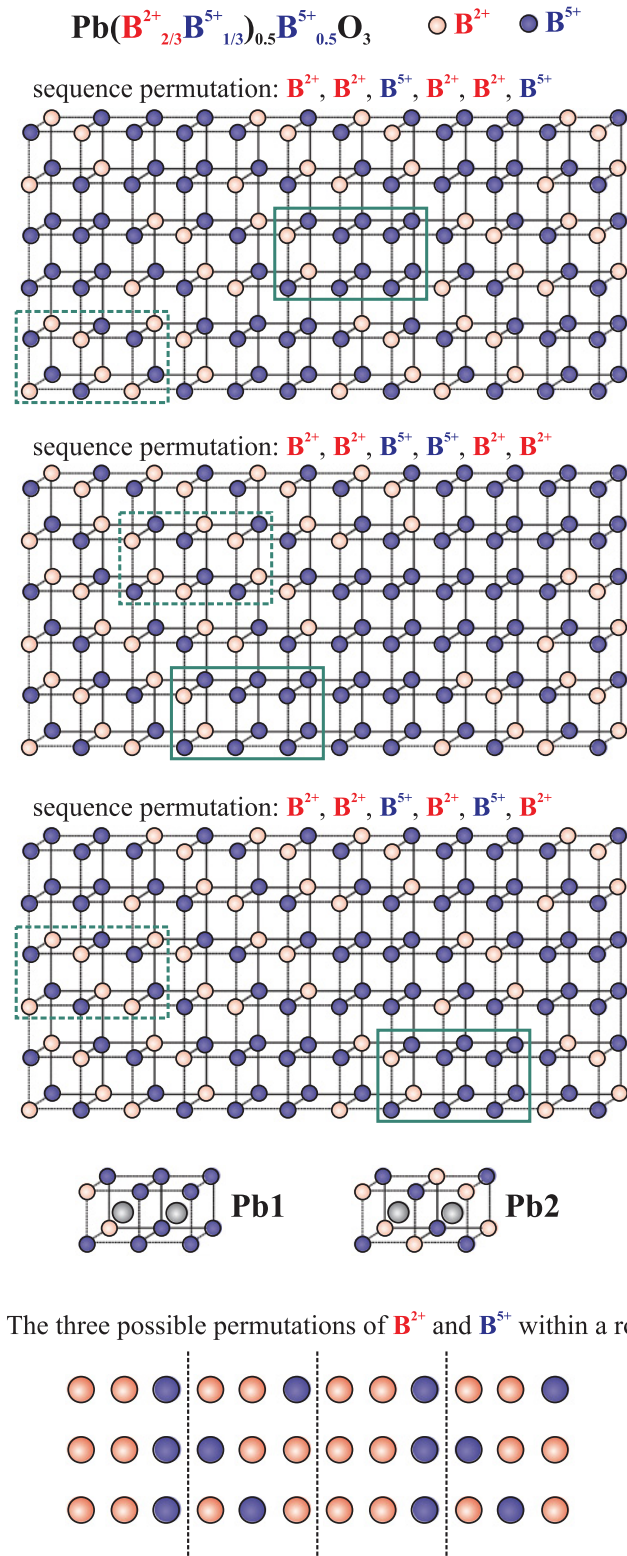
$$Pb(B^{2+}_{2/3}B^{5+}_{1/3})_{0.5}B^{5+}_{0.5}O_3 \qquad \circ\ B^{2+} \quad \bullet\ B^{5+}$$

sequence permutation: B^{2+}, B^{2+}, B^{5+}, B^{2+}, B^{2+}, B^{5+}

sequence permutation: B^{2+}, B^{2+}, B^{5+}, B^{5+}, B^{2+}, B^{2+}

sequence permutation: B^{2+}, B^{2+}, B^{5+}, B^{2+}, B^{5+}, B^{2+}

 Pb1 Pb2

The three possible permutations of B^{2+} and B^{5+} within a row

FIG. 5. (Color online) Examples of ordered B-cation configurations of type Pb $B'_{0.5}B''_{0.5}O_3$, where B' is randomly occupied by 2/3 B^{2+} and 1/3 B^{5+} cations, while B' is exclusively occupied by B^{5+}. As a result, $Pb(B^{2+}_{2/3}B^{5+}_{1/3})_{0.5}B^{5+}_{0.5}O_3$ regions are formed with two Pb states distinguished by the surrounding B cations. The solid bold rectangles mark structural units that comprise Pb1 ions; the dashed bold rectangles mark structural units that comprise Pb2 ions. The sequence permutations refer to the B^{2+} and B^{5+} cations occupying the B' site.

which are off-center displaced, should give rise to a peak in the $\bar{Z}(XX)Z$ spectrum. Statistically, Pb1 states are expected to be twice less than Pb2 states. We assign the lower-wave-number peak ($\sim$45 cm^{-1}) and higher-wave-number peak ($\sim$57 cm^{-1}) in the $\bar{Z}(XY)Z$ spectra to vibrational states of Pb1 and Pb2 ions, respectively, because of two reasons: (i) the lower-wave-number peak is suppressed when diluting PZN with PT,[23] indicating that this peak is related to the less abundant Pb states in the $Pb(B^{2+}_{2/3}B^{5+}_{1/3})_{0.5}B^{5+}_{0.5}O_3$ regions; (ii) for $PbB^{3+}_{0.5}B^{5+}_{0.5}O_3$ relaxors the "allowed" $\bar{Z}(XY)Z$ peak is always positioned at a higher wave number than the "forbidden" $\bar{Z}(XX)Z$ peak.[5,31,34] Based on the comparison to the frequencies of phonon modes measured by inelastic neutron scattering, the peak near 45 cm^{-1} has been previously assigned to disorder-induced scattering from $Pm\bar{3}m$ zone-boundary transverse acoustic modes.[35] Transferring vibrational energy from acoustic to optical phonon branches when the structure is doubled is highly plausible and coupling between acoustic and optical phonons may occur, but this process should be related with the Pb1 state characteristic of $PbB'_{1/3}B''_{2/3}O_3$ systems because, as mentioned above, a doublet in the $\bar{Z}(XY)Z$ spectrum is not observed for the high-temperature state of $PbB'_{0.5}B''_{0.5}O_3$ relaxors. Taniguchi *et al.*[30] have ascribed the peak observed at 45 cm^{-1} as stemming from the F_{2g} mode due to the orientational dependence of the intensity of this peak, without discussing the second peak near 57 cm^{-1}, although both peaks show exactly the same orientational dependence typical of cubic F_{2g} modes.[30] Actually, the high-quality polarized Raman data presented in Ref. 30 clearly support our suggestion that the doublet 45–57 cm^{-1} observed at high temperatures in $\bar{Z}(XY)Z$ spectra of $PbB'_{1/3}B''_{2/3}O_3 - x$PT arises from two vibrational states of Pb atoms in a cubic double-perovskite $Fm\bar{3}m$ structure related to the $PbB'_{1/3}B''_{2/3}O_3$ component.

2. Temperature evolution of phonon modes

The temperature dependences of the positions, FWHMs, and integrated-intensity ratio $I_{45\text{cm}^{-1}}/(I_{45\text{cm}^{-1}} + I_{57\text{cm}^{-1}})$ of the Raman signals near 50 cm^{-1} for PZN-0.1PT are shown in Fig. 6. For this compound the Pb1-type ions are surrounded predominantly by Nb^{5+}, while Pb2-type ions are surrounded by both Zn^{2+} and Nb^{5+}. Titanium is expected to be randomly distributed in the cationic environments of both Pb1 and Pb2 ions, i.e., its presence is insufficient for the distinction of the two states of Pb ions. As can be seen in Fig. 6, all characteristic temperatures can be determined from the temperature evolution of the "forbidden" $\bar{Z}(XX)Z$ Raman signal: The Burns temperature $T_B = 730$ K and the intermediate temperature $T^* = 525$ K are revealed by the local maxima in the FWHM as a function of temperature [Fig. 6(c)], $T_{C1} = 450$ K is marked by the kink in the FWHM [Fig. 6(c)], and $T_{C2} = 350$ K is indicated by the splitting of this peak [Figs. 3, 6(a), 6(c), and 6(e)] due to lowering of the point symmetry. The values determined from the Raman data are in excellent agreement with the characteristic temperatures measured by acoustic emission.[20] In the temperature range from 850 K to $T_{C2} = 350$ K the frequency of the $\bar{Z}(XX)Z$ peak changes very slightly, but seemingly the peak hardens below T^* [Fig. 6(a)].

The intermediate temperature $T^* = 525$ K is much better shown by the drop in the temperature dependence of the

PZN-0.1PT
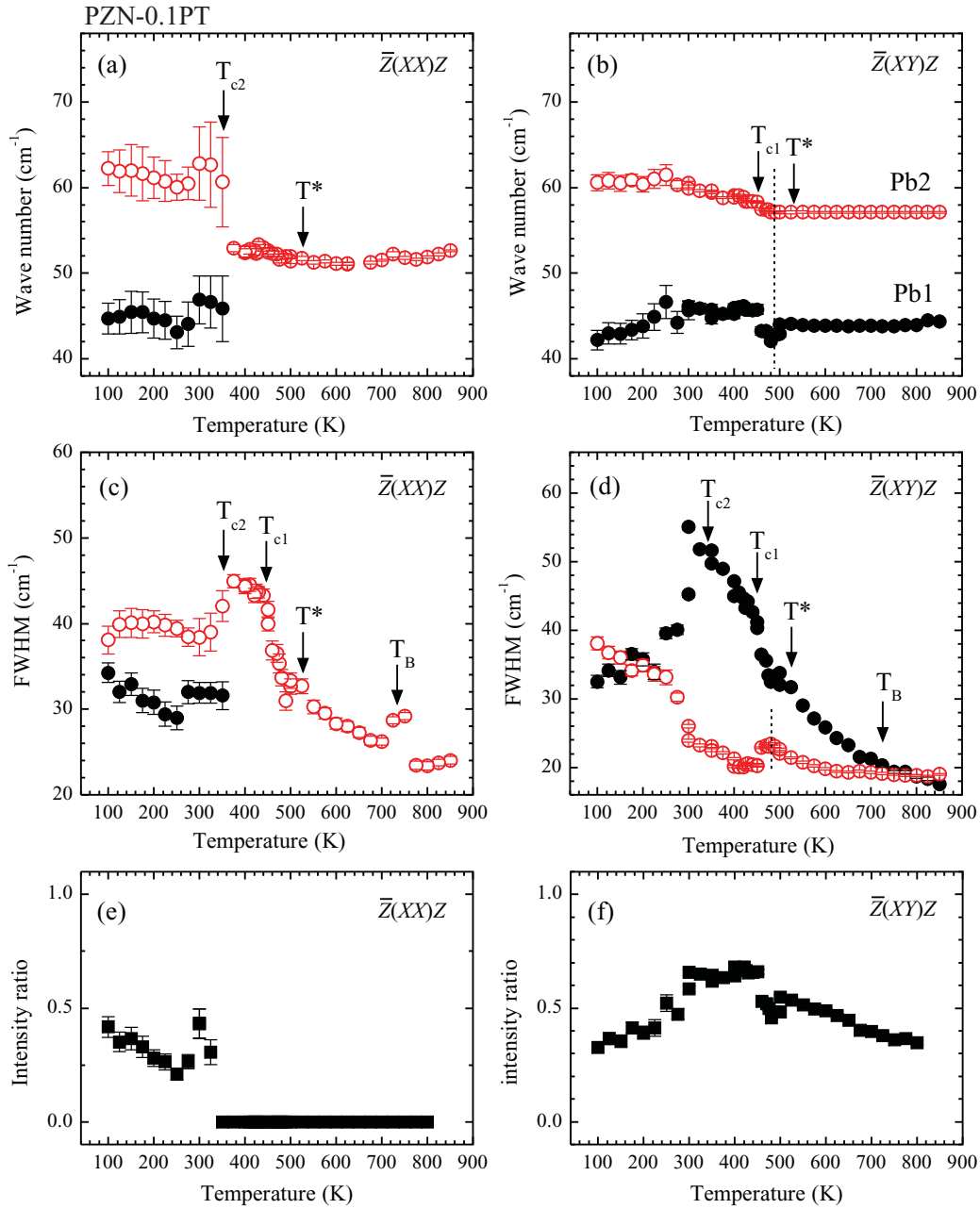

FIG. 6. (Color online) Temperature dependence of the positions, FWHMs, and intensity ratio $I_{45cm^{-1}}/(I_{45cm^{-1}} + I_{57cm^{-1}})$ of the Raman peaks of PZN-0.1PT related to the Pb-localized F_{2g} mode of the prototype doubled structure ($Fm\bar{3}m$). At high temperatures (above T_{C2}) the solid and open circles correspond to the two vibrational Pb states: Pb1 surrounded predominantly by Nb and Pb2 surrounded by both Zn and Nb; Ti can be in the surroundings of both Pb1 and Pb2 atoms. Below T_{C2} two peaks are observed in both $\bar{Z}(XX)Z$ and $\bar{Z}(XY)Z$ due to the lowering of the point symmetry of the average structure.

FWHM of the peak near 260 cm^{-1} (Fig. 7). This peak is related to the infrared-active B-cation-localized F_{1u} mode of the prototype $Fm\bar{3}m$ structure, whose Raman activity results from the presence of off-centered B-cation displacements.[29,31] It should be underlined that so far a sharp decrease in the width of the Raman peak near 260 cm^{-1} at T^* has been reported for relaxors of type $(Pb,A'')B'_{0.5}B''_{0.5}O_3$, $PbB'_{0.5}(B''_{1-x}B'''_x)_{0.5}O_3$, and $Pb(B'_{0.5}B''_{0.5})_{1-x}B'''_xO_3$.[5,31,34] The fact that the same is observed for a compound of type $PbB'_{1/3}B''_{2/3}O_3-x$PT emphasizes the universal character of

the transformation processes occurring at T^*, namely, strongly enhanced coherence between off-centered displacements of B-site cations (regardless of their multiple type), leading to stable PNRs with a mean size and lifetime considerably larger than the mean size and lifetime of polar clusters that appear at T_B.

All characteristic temperatures can also be deduced by comparing the temperature dependence of the FWHM of the peaks near 45 and 57 cm^{-1} in the $\bar{Z}(XY)Z$ spectra [Fig. 6(d)]. Above T_B the two "cubic" peaks related to Pb1 and Pb2 states
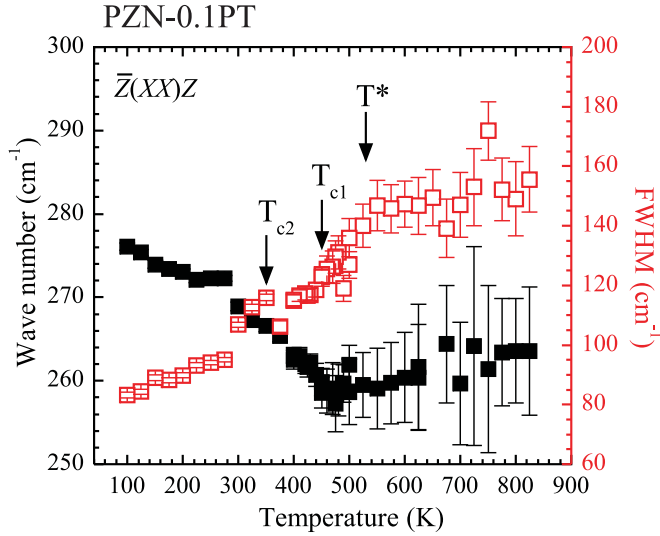
FIG. 7. (Color online) Temperature dependence of the position (solid squares) and FWHM (open squares) of the $\bar{Z}(XX)Z$ peak of PZN-0.1PT related to the B-cation-localized F_{1u} mode of the prototype $Fm\bar{3}m$ structure.

FIG. 8. (Color online) Depolarization ratio $\eta = I_{XY}/(I_{XY} + I_{XX})$ of the Raman band between 700 and 900 cm^{-1} for PZN-0.1PT, where I_{XY} and I_{XX} are the integrated intensities of the corresponding peaks in $\bar{Z}(XY)Z$ and $\bar{Z}(XX)Z$ geometry; the curve represents a Boltzmann fit to the experimental points with a midpoint of the slope $x_0 = 293 \pm 5$ K.

have nearly the same widths, but at T_B the Raman peak at 45 cm^{-1} associated with Pb1 ions (surrounded predominantly by Nb^{5+}) begins to broaden much more strongly than the $\bar{Z}(XY)Z$ peak near 57 cm^{-1}. Upon further cooling the peak near 45 cm^{-1} continues to broaden until T_{C2} is reached, but the rate of broadening changes at T^* and at T_{C1}. Below 250 K the widths of the peaks near 45 and 57 cm^{-1} observed in $\bar{Z}(XY)Z$ geometry are similar, indicating that the two Pb states (distinguished by chemical environment) are in coherence concerning local structural distortions. At 250 K the depolarization of the parallel- and cross-polarized spectra measured when the incident light polarization is parallel to the cubic edge reaches a constant value (see Fig. 8), indicating a saturation of structural transformations. Interestingly, the FWHM of the peak near 57 cm^{-1}, related to Pb2 atoms (surrounded by both Zn^{2+} and Nb^{5+}), has a local maximum at 485 K, which is between T_{C1} and T^* [Fig. 6(d)]. At the same temperature the frequency of this peak begins to harden and the frequency of the peak related to Pb1 has a slight minimum [see Fig. 6(b)]. These features further emphasize the fact that the formation of ferroelectric long-range order in PZN-0.1PT is a multistep process. At $T > T_B$ the intensity ratio $I_{45\text{cm}^{-1}}/(I_{45\text{cm}^{-1}} + I_{57\text{cm}^{-1}})$ observed in $\bar{Z}(XY)Z$ geometry is ~ 0.35 [see Fig. 6(e)]. This value matches very well the fraction of cation pairs B^{5+}-B^{5+}, as deduced from the general formula Pb(B$^{2+}_{2/3}$B$^{5+}_{1/3}$)$_{0.5}$B$^{5+}_{0.5}$O$_3$. The intensities of the $\bar{Z}(XY)Z$ peaks near 45 and 57 cm^{-1} change with temperature due to the development of ferroic order. It is well known that near a phase transition the integrated intensities of the low-energy hard phonon modes have a maximum due to the structural instability and their coupling with the flip mode representing the fluctuations of the structure between instantaneous configurations.[38,39] Indeed, the intensity ratio $I_{45\text{cm}^{-1}}/(I_{45\text{cm}^{-1}} + I_{57\text{cm}^{-1}})$ measured in $\bar{Z}(XY)Z$ geometry increases upon cooling, has a broad
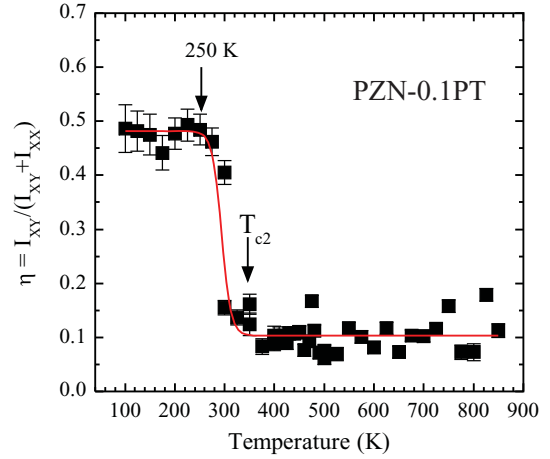
maximum in the temperature range between T_{C1} and T_{C2}, and then decreases upon further cooling.

The assignment of the Raman scattering in the spectral range 100–200 cm^{-1} is hampered by the multiple chemical and structural inhomogeneity existing in PZN-0.1PT. By analogy with other relaxor systems the peaks near 100 and 130 cm^{-1} might be related to the infrared Pb-BO$_3$ translation F_{1u} mode characteristic of both single ($Pm\bar{3}m$) and double ($Fm\bar{3}m$) perovskite structure [Ref. 31 and references therein], which is activated in the Raman spectra due to polar cation shifts. Hence, these peaks might account for the dynamical coupling between off-centered displacements of Pb and B cations in PNRs. The two peaks harden in frequency close to the C-T phase transition (see Fig. 9), similarly to the peak near 260 cm^{-1} (Fig. 7). Also, both peaks sharpen below T_{C1} as the FWHM of the peak near 100 cm^{-1} has a wide maximum centered at T^*, while the peak at 130 cm^{-1} is broadened in a wider temperature range between T_B and above T_{C1} (Fig. 9).

Based on the observed spectral changes, one can propose the following scenario for the transformation processes that occur upon cooling in PZN-0.1PT. Due to the affinity of Pb^{2+} to form lone pair electrons, the structure possesses intrinsic off-centered displacements of Pb ions which are surrounded by locally ordered Zn and Nb. At $T_B = 730$ K the off-center shifted Pb ions drive the surrounding B cations to coherently shift away from the octahedral center, which results in a nucleation of small polar clusters. The ferroelectrically active Nb^{5+} cations are expected to be more involved in this process as compared to Zn^{2+}, thus leading to a significant distortion of the B-site cation shell of the Pb cations surrounded predominantly by Nb^{5+}. Consequently, below T_B Pb1 cations can have some room for tiny off-center shifts though the strong electrostatic repulsive interactions. This causes a displacive disorder of Pb1 as revealed by the strong increase in the FWHM of the peak at 45 cm^{-1} [see Fig. 6(d)]. Upon cooling, the width of this peak further increases due to the increasing distortion in the Nb^{5+} shells of Pb1 ions. Hence, the rate of
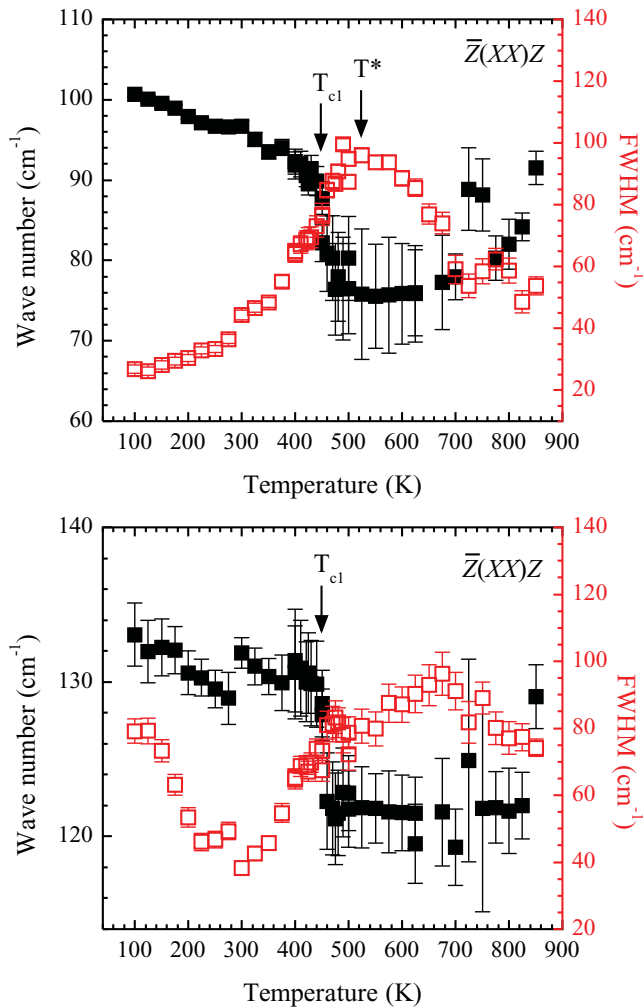
FIG. 9. (Color online) Temperature dependence of the position (solid squares) and FWHM (open squares) of the $\bar{Z}(XX)Z$ peaks of PZN-0.1PT near 100 cm^{-1} (upper plot) and 130 cm^{-1} (bottom plot).

the width increase follows the enlargement of the fraction of polar clusters comprising off-centered Nb atoms. The small plateau near T^* of the FWHM for the 45-cm^{-1} peak [Fig. 6(d)] reveals that at this characteristic temperature the dominant transformation process is coupling between polar clusters rather than further nucleation of polar species. Titanium is also ferroelectrically active; Ti^{4+} cations can displace along the cubic $\langle 111 \rangle$ direction, following the displacement direction of the major cations in the solid solution[40] or they can shift along the cubic $\langle 001 \rangle$ to stabilize the second-order Jahn-Teller off-centering of Ti in the presence of a stereochemically active lone pair on the Pb ion.[41] Direct evidence for the state of Ti cations cannot be gained from the Raman data presented here, as peaks arising solely from Ti vibrations cannot be distinguished. This suggests, however, one-mode behavior for the B-site system and hence one can speculate that initially Ti cations follow the rhombohedral distortion typical of PNRs.[2,17] Probably, in the temperature range between T^* and T_{C1}, where the peak at 57 cm^{-1} has a maximum of the width [Fig. 6(d)] and starts to harden [Fig. 6(b)], tetragonal-type polar atomic arrangements prevail over rhombohedral polar clusters and

begin to merge to evolve in long-range ordered tetragonal domains at T_{C1}.

It is worth noting that the development of tetragonal domains does not influence the depolarization ratio of the parallel- and cross-polarized spectra measured when the incident light polarization is along the cubic edge [$\bar{Z}(XX)Z$ and $\bar{Z}(XY)Z$ spectra] because the tetragonal axes are along the cubic axes and do not incline to the directions of the polarization of the incident and scattering light. However, as can be seen in Fig. 4, the occurrence of tetragonal domains is clearly revealed by the depolarization of the spectra measured when the incident light polarization is along the cubic face diagonal [$\bar{Z}(X'X')Z$ and $\bar{Z}(X'Y')Z$ spectra] because in this case the tetragonal domains are oriented at 45° with respect to the polarization of the incident and scattered light and hence, contribute equally to the parallel- and cross-polarized spectra. The $\bar{Z}(XX)Z$ and $\bar{Z}(XY)Z$ spectra would depolarize if rhombohedral, orthorhombic (with a unit cell rotated by 45° with respect to the cubic cell), or monoclinic (triclinic) domains are formed. By this reason the $\bar{Z}(XX)Z$ and $\bar{Z}(XY)Z$ are depolarized below T_{C2}. An attempt was made to determine the predominant type of ferroelectric domains in the structure by measuring the angular dependence of the depolarization of the Raman band near 700–900 cm^{-1} at room temperature. Since no extrema at every 45° were detected, one can argue that the structural distortion is monoclinic (or triclinic) rather than orthorhombic or rhombohedral. At temperatures below 250 K the spectra measured in all four scattering geometries become almost the same (see Fig. 4). This indicates that regardless of the chemical inhomogeneity, the structure becomes homogeneous with respect to the ferroic distortion developed on the length scale of sensitivity of Raman spectroscopy, i.e., within a few unit cells.

C. Raman scattering of Ru-doped PZN-0.1PT

Ruthenium is a mixed-valence 4d transition element with the ability to exhibit different oxidation states, e.g., Ru^{3+}, Ru^{4+}, and Ru^{5+}.[42] The 4d transition ions are known to be more covalently bound to oxygen than 3d transition ions (like Ti^{4+}) and give rise to a strong octahedral crystal field.[42] Besides, Ru^{4+} can be in a low-spin magnetic or in a high-spin nonmagnetic state.[43,44] Thus, the incorporation of Ru even in small concentrations may considerably influence the structural transformations. It has been previously shown that in PZN-0.1PT Ru ions predominantly replace Ti ions with a mean valence of Ru slightly below 4+.[15] Electron paramagnetic resonance spectroscopy revealed two types of paramagnetically active Ru centers in the structure of PZN-0.1PT : Ru^{3+} and Ru^{5+}.[15] At room temperature Ru^{3+} prevails over Ru^{5+}, leading to immobilization of the domain walls and hardening of the hysteresis loops; cooling from 300 to 100 K leads to Ru^{3+}→Ru^{5+} transformation.[15]

The $\bar{Z}(XX)Z$ and $\bar{Z}(XY)Z$ Raman spectra of PZN-0.1PT : Ru collected between 850 and 100 K are shown in Fig. 10. The Raman spectra exhibit the same general features observed for the pure compound. As in the case of the undoped compound, at high temperatures there are two peaks near 50 cm^{-1} in the $\bar{Z}(XY)Z$ spectra and only one peak in the $\bar{Z}(XX)Z$ spectra. Therefore, the addition of Ru does not
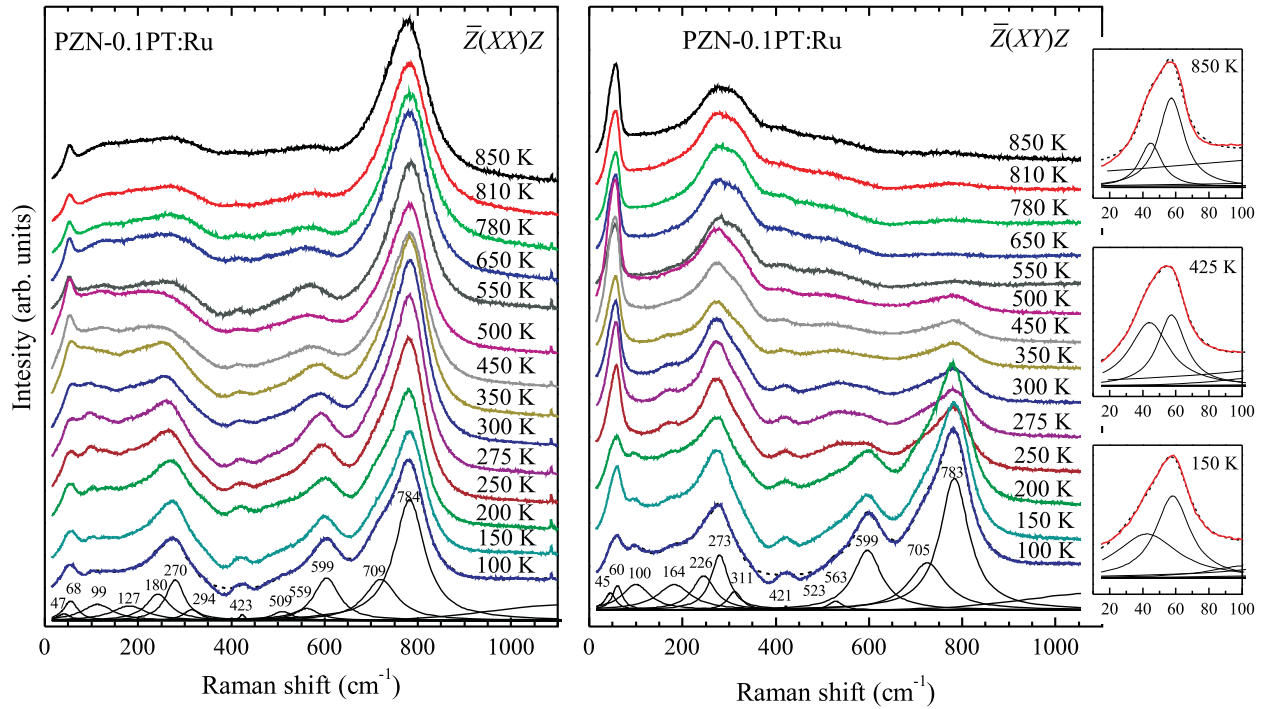
FIG. 10. (Color online) Parallel- $\bar{Z}(XX)Z$ and cross- $\bar{Z}(XY)Z$ polarized Raman scattering of Ru-doped PZN-0.1PT collected at different temperatures in the range 100–850 K; thin lines represent the fitting Lorentzians used for 100 K. An additional Gaussian centered near 1150 cm^{-1} was used for this compound to account for the continuum photoluminescence background. Insets on right show on an enlarged scale the band near 50 cm^{-1} measured in $\bar{Z}(XY)Z$ geometry (red bold curves), the corresponding fitting Lorentzians (thin curves), and resultant spectrum profiles (black dashed curves).

affect the existence of the two "cubic" states of Pb. Upon cooling, the peaks related to polar distortions enhance and sharpen. The depolarization of the spectra is clearly seen below 200 K, at which temperature a splitting of the $\bar{Z}(XX)Z$ peak near 50 cm^{-1} is also resolved. These observations demonstrate the development of M_C-type domains, indicating that Ru doping does not move the compound away from the MPB. The temperature dependence of the depolarization ratio (Fig. 11) shows that the depolarization of the spectra of PZN-0.1PT : Ru takes place over a temperature range from ∼300 to 150 K, which is larger than the corresponding temperature range 350–250 K for pure PZN-0.1PT. Ru doping decreases T_{C2} with ∼50 K, as indicated by the beginning of the stepwise increase in the depolarization ratio (compare Figs. 8 and 11). In addition, the temperature dependence of the depolarization ratio for PZN-0.1PT : Ru does not have such a steep inclination as for pure PZN-0.1PT, revealing a more diffuse development of M_C-type domains as compared to the pure compound. The incorporation of a fourth type of cation on the B site resulted in an additional broadening of the Raman signals and this unfortunately hindered the rational fitting of the spectra above 600 K. Because of the obtained large uncertainties in the fitting parameters for the Raman signals between 100 and 400 cm^{-1}, we restricted the analysis to the Raman signals related to the Pb-localized F_{2g} mode of the prototype structure (see Fig. 12). As in the case of pure PZN-0.1PT, the Burns temperature can be determined from the change in the FWHM of the peaks seen in $\bar{Z}(XY)Z$ geometry [Fig. 12(d)]. According to these data, T_B for PZN-0.1PT:Ru is just below 700 K, i.e., with

∼30 K lower than for PZN-0.1PT. This is most probably due to the presence of local structural distortions associated with Ru-doping centers, which interferes with the coupling of polar displacements of the host-matrix cations. By contrast to the pure compound, T_B is not clearly marked in the temperature dependence of the width of the $\bar{Z}(XX)Z$ peak [Fig. 12(c)],
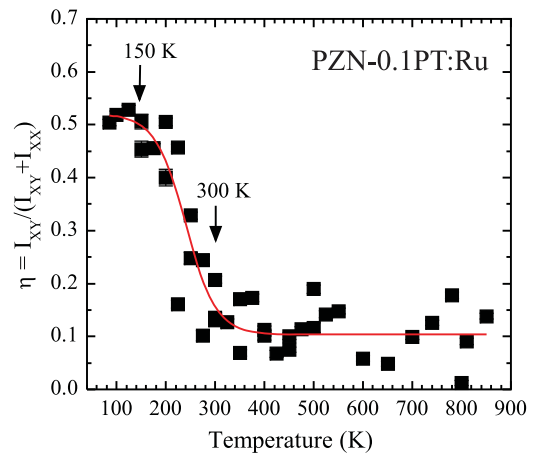

FIG. 11. (Color online) Depolarization ratio $\eta = I_{XY}/(I_{XY}+I_{XX})$ of the Raman band between 700 and 900 cm^{-1} for Ru-doped PZN-0.1PT, where I_{XY} and I_{XX} are the integrated intensities of the corresponding peaks in $\bar{Z}(XY)Z$ and $\bar{Z}(XX)Z$ geometry; the curve represents a Boltzmann fit to the experimental points with a midpoint of the slope $x_0 = 240 \pm 11$ K.
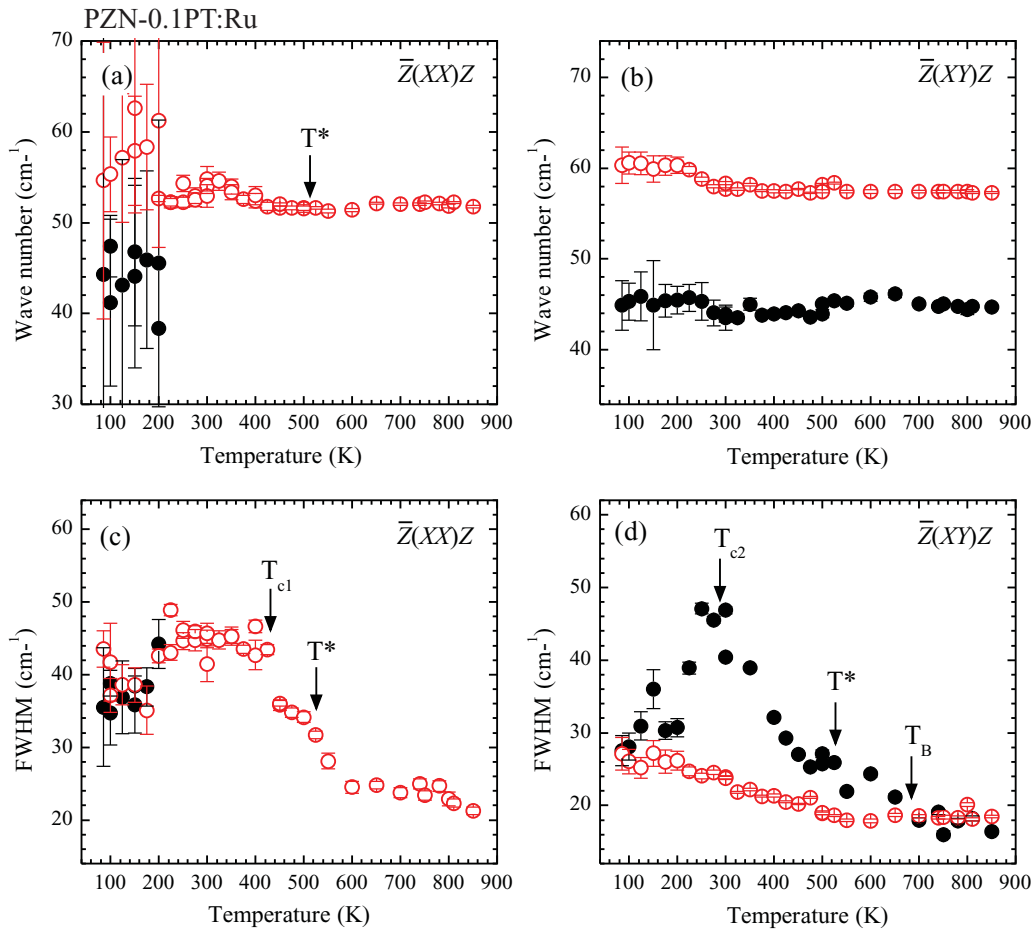
FIG. 12. (Color online) Temperature dependence of the positions and FWHMs of the Raman peaks of Ru-doped PZN-0.1PT related to the Pb-localized F_{2g} mode of the prototype doubled structure ($Fm\bar{3}m$). At high temperatures (above T_{C2}) the solid and open circles correspond to the two vibrational Pb states: Pb1 surrounded predominantly by Nb and Pb2 surrounded by both Zn and Nb; Ti can be in the surroundings of both Pb1 and Pb2 atoms. Below T_{C2} two peaks are observed in both $\bar{Z}(XX)Z$ and $\bar{Z}(XY)Z$ due to the lowering of the point symmetry of the average structure.

suggesting that doping smears out the transformation process. The same is valid for the intermediate temperature T^*, which can be deduced to be ∼525 K by the broad local maximum in the FWHM and the subtle hardening of the $\bar{Z}(XX)Z$ peak [Figs. 12(c) and 12(a)] as well as the kink in the FWHM of the $\bar{Z}(XY)Z$ peak at 45 cm^{-1} [Fig. 12(d)]. Above 500 K the B-cation-localized mode near 260 cm^{-1} is very broad and hardly resolvable from the nearest overlapping Raman signals, which also indicates that T^* is near 500–525 K. The C-T phase transition temperature T_{C1} can be found from the kink in the temperature dependence of the FWHM of the $\bar{Z}(XX)Z$ peaks [Fig. 12(c)], in the same manner as for pure PZN-0.1PT. The T-M phase transition temperature T_{C2} is, however, more difficult to determine. According to the depolarization ratio (Fig. 11), T_{C2} is ∼300 K; however, the maximum in the FWHM of the peak near 45 cm^{-1} [Fig. 12(d)] is ∼ 280 K, whereas the splitting in the $\bar{Z}(XX)Z$ peak arising from Pb-localized vibrations is resolved only at 200 K. This underlines the diffuseness of the structural transformation from tetragonal to monoclinic. Interestingly, even a very small

substitution of Ru for Ti (Ru/Ti ratio = 0.02) considerably influences the development of ferroelectric long-range order in the overall structure. It appears that Ru favors the tetragonal distortion over a wider temperature range. As mentioned above, in PZN-0.1PT Ru is in third-, fourth-, and fifth-valence substitutes for Ti^{4+} and at room temperature there is a surplus of Ru^{3+}.[15] Octahedra deformed along one of the BO$_6$ fourfold axes are energetically favorable for Ru^{4+}.[44,45] Ru^{3+} cations are also associated with tetragonally elongated octahedra, without off-centering of the cation, whereas Ru^{5+} cations form with the nearest oxygen ions strongly off-centered axially perturbed octahedral.[42] Seemingly, the predominance of Ru-doping centers related to local tetragonal distortions holds down the formation of monoclinic domains and thus shifts the T-M transition of the whole system to lower temperatures. However, upon cooling the host perovskite structure eventually develops a monoclinic-type ferroelectric order and, in turn, forces the Ru doping ions to change the valence from 3+ to 5+ because strongly off-centered axially perturbed BO$_6$ octahedra better match Ru^{5+} as compared to Ru^{3+}.

D. A plausible structural state of Pb-based B-site complex perovskite-type relaxors

The formation of PNRs is usually considered in terms of chemically B-site ordered and disordered regions as seen by x-ray, neutron, or electron diffraction. The predominant opinion is still that dynamical polar nanoregions are associated exclusively with chemically B-site disordered regions, although Raman scattering clearly indicates that all Pb-based B-site complex perovskite-type relaxor systems have lattice dynamics typical of a doubled structure, i.e., typical of B-site ordered regions. Modes existing only in a doubled perovskite structure are strongly influenced by the formation of polar order as demonstrated in this paper and in Refs. 5, 31, and 34, regardless of the stoichiometry on the B site. This suggests that on the mesoscopic scale one can hardly discriminate chemically ordered from chemically disordered regions and polar regions simply penetrate through the structure. Putting it another way, fine-scale atomic arrangements that are chemically 1:1 ordered exist also in that fraction of the material seen by diffraction as chemically disordered and therefore, regions exhibiting polarization should always possess local chemical 1:1 B-site order. This statement is supported by x-ray absorption spectroscopic data revealing a surprisingly high degree of local 1:1 ordering of the B-site cations (on the length scale of $\sim$5 Å) in relaxor-based solid solutions[40] exhibiting no long-range chemical B-site order. However, chemical 1:1 B-site order favors antiferroelectric off-center displacements of the nearest Pb and O ions,[46] meaning that there should be antiferroelectric-type coupling inside polar regions. This, at first glance, incongruous statement actually has a very simple and elegant explanation: *ferrielectricity*, due to the coexistence of ferroelectric and antiferroelectric coupling in ferroic regions. Local chemical 1:1 B-site cation order favors antipolar shifts of the Pb atoms. On the other hand, off-centering of Pb cations favors polar displacements of the corresponding nearest ferroelectrically active B cations and hence, small polar BO_3-Pb species are formed in the structure. The faults of the chemical B-site order modulate the off-center shifts of the Pb cations and, consequently the dipoles associated with polar BO_3-Pb atomic species, which on the mesoscopic scale leads to *frustrated ferrielectric* order. These arguments are not valid for Ba-based systems, because Ba does not form stereochemically active lone pairs, i.e., it has no affinity to displace off-center and therefore antiferroelectric coupling inside PNRs is very unlikely. This principle difference between the nature of ferroic order in PNRs might be the key reason to explain why Pb-based relaxor systems have considerably stronger response functions as compared to Ba-based relaxor systems.

The assumption that polar nanoregions in Pb-based perovskite-type relaxor ferroelectrics might be ferrielectric in nature rather than ferroelectric is supported by the fact that pressure suppresses the coupling between off-centered Pb and B-site cations and the polar B-cation shifts, thus favoring the establishment of antiferrodistortive long-range order, which is developed from ferroic species already existing at ambient conditions.[31,47,48] In addition, for chemically disordered $PbSc_{0.5}Ta_{0.5}O_3$ a phase transformation attributed to the development of modulated antiferrodistortive order slightly above the temperature of the dielectric-permittivity maximum was observed by acoustic emission.[49] Incommensurate modulated antiferrodistortive order was observed by transmission electron microscopy in $PbSc_{0.5}Ta_{0.5}O_3$ single crystals with a high degree of chemical B-site order.[50] Local antiferroelectric order was also deduced from x-ray diffuse scattering data on $PbSc_{0.5}Nb_{0.5}O_3$.[51] A ferrielectric type of the nanoscale polar order in relaxors is also an alternative plausible explanation for the V-type dependence of the dielectric-permittivity maximum temperature on an external electric field observed for PMN-0.33PT by acoustic emission,[52] which is typical of antiferroelectric order. The T_C for PMN-0.33PT as detected by XRD shows the expected gradual increase with increasing the electric field,[52] but XRD probes the ferroic long-range order, i.e., indicates the temperature at which normal ferroelectric domains appear, whereas acoustic emission measures the response of the whole system, i.e., it is sensitive also to structural transformations related to PNRs.

IV. CONCLUSIONS

The Raman peaks related to the cubic Pb-localized F_{2g} mode, which exists only in a doubled-perovskite structure, are highly sensitive to the nucleation and development of polar order. By following the temperature evolution of the spectral parameters of these peaks, one can identify all characteristic temperatures typical of PZN-0.1PT. The two peaks near 50 cm^{-1} observed in the high-temperature $\bar{Z}(XY)Z$ spectra of PZN-xPT are attributed to two distinct cubic states of Pb ions in regions with a local chemical order of the type $Pb(B_{2/3}^{2+}B_{1/3}^{5+})_{0.5}B_{0.5}^{5+}O_3$: (i) less abundant Pb1 ions surrounded by Nb^{5+} and (ii) more abundant Pb2 ions surrounded by both Zn^{2+} and Nb^{5+}. The temperature dependence of the Raman spectra of PZN-0.1PT indicates that off-centered Pb2 ions induce coherent polar shifts of ferroelectrically active B cations, which in turn facilitates the off-centering of Pb1 ions. Also, Raman data suggest the predominance of monoclinic-type ferroelectric domains in the room temperature structure of as-synthesized (unpoled) crystals.

A low degree of B-site doping with mixed-valence elements like Ru can substantially influence the development of ferroelectric long-range order in PZN-xPT solid solutions close to the MPB. This phenomenon is most probably due to the different preferred types of local octahedral distortion associated with the different valence states of the doping cations. The incorporation of Ru into the structure of PZN-0.1PT slightly decreases T_B, smears the transformation processes near T^*, and favors the long-range tetragonal order over a wide temperature range, shifting the T-M transition to lower temperatures.

An assumption is made that Pb-based B-site complex perovskite-type relaxor systems might be nanoscale frustrated ferrielectrics.

*Corresponding authors: boriana.mihailova@uni-hamburg.de; naemi.waeselmann@mineralogie.uni-hamburg.de

[1] W. S. Chang, L. C. Lim, F.-T. Wang, C.-M. Hsieh, and C.-S. Tu, J. Phys. Condens. Matter **20**, 395229 (2008).

[2] D. La-Orauttapong, J. Toulouse, J. L. Robertson, and Z. G. Ye, Phys. Rev. B **64**, 212101 (2001).

[3] I. K. Jeong and J. K. Lee, App. Phys. Lett. **88**, 262905 (2006).

[4] J. Toulouse, F. Jiang, O. Svitelski, W. Chen, and Z. G. Ye, Phys. Rev. B **72**, 184106 (2005).

[5] B. Mihailova, B. J. Maier, C. Paulmann, T. Malcherek, J. Ihringer, M. Gospodinov, R. Stosch, B. Güttler, and U. Bismayer, Phys. Rev. B **77**, 174106 (2008).

[6] Y. Yan, S. J. Pennycook, Z. Xu, and D. Viehland, Appl. Phys. Lett. **72**, 3145 (1998).

[7] M. L. Mulvihill, S. E. Park, G. Risch, Z. Li, K. Uchino and T. R. Shrout, Jpn. J. Appl. Phys. **35**, 3984 (1996).

[8] S. E. Park and T. R. Shrout, J. Appl. Phys. **82**, 1804 (1997).

[9] D. La-Orauttapong, B. Noheda, Z. G. Ye, P. M. Gehring, J. Toulouse, D. E. Cox, and G. Shirane, Phys. Rev. B **65**, 144101 (2002).

[10] B. Noheda, D. E. Cox, G. Shirane, S. E. Park, L. E. Cross, and Z. Zhong, Phys. Rev. Lett. **86**, 3891 (2001).

[11] R. Guo, L. E. Cross, S. E. Park, B. Noheda, D. E. Cox, and G. Shirane, Phys. Rev. Lett. **84**, 5423 (2000).

[12] D. Vanderbilt and M. H. Cohen, Phys. Rev. B **63**, 094108 (2001).

[13] Y. Uesu, M. Matsuda, Y. Yamada, K. Fujishiro, D. E. Cox, B. Noheda, and G. Shirane, J. Phys. Soc. Jpn. **71**, 960 (2002).

[14] S. Madeswaran, S. V. Rajasekaran, R. Jayavel, S. Ganesamoorthy, and G. Behr, Mater. Sci. Eng. B **120**, 32 (2005).

[15] T. Scholz, B. Mihailova, G. A. Schneider, N. Pagels, J. Heck, T. Malcherek, R. P. Fernandes, V. Marinova, M. Gospodinov, and U. Bismayer, J. Appl. Phys. **106**, 074108 (2009).

[16] G. Xu, Z. Zhong, H. Hiraka, and G. Shirane, Phys. Rev. B **70**, 174109 (2004).

[17] D. La-Orauttapong, J. Toulouse, Z. G. Ye, W. Chen, R. Erwin, and J. L. Robertson, Phys. Rev. B **67**, 134110 (2003).

[18] G. Xu, J. Phys. Soc. Jpn. **79**, 011011 (2010).

[19] O. Svitelskiy, D. La-Orauttapong, J. Toulouse, W. Chen, and Z. G. Ye, Phys. Rev. B **72**, 182106 (2005).

[20] E. Dul'kin, M. Roth, P. E. Janolin, and B. Dkhil, Phys. Rev. B **73**, 012102 (2006).

[21] J. H. Ko, D. H. Kim, and S. Kojima, Phys. Rev. B **77**, 104110 (2008).

[22] J. Toulouse, Ferroelectrics **369**, 203 (2008).

[23] M. Iwata, Y. Hasegawa, R. Aoyagi, M. Maeda, N. Wakiya, H. Suzuki, and Y. Ishibashi, Ferroelectrics **378**, 84 (2009).

[24] J. Cheng, Y. Yand, Y. H. Tong, S. B. Lu, J. Y. Sun, K. Zhu, Y. L. Liu, G. G. Siu, and Z. K. Xu, J. Appl. Phys. **105**, 053519 (2009).

[25] M. El Marssi and H. Dammak, Solid State Commun. **124**, 487 (2007).

[26] C. Paulmann and T. Malcherek, Hasylab Annual Report, Part I, 1399 (2006).

[27] T. R. Welberry and D. Goossens, J. Appl. Cryst. **41**, 606 (2008).

[28] M. Paściak, M. Wołcyrz, and A. Pietraszko, Phys. Rev. B **76**, 014117 (2007).

[29] B. Mihailova, U. Bismayer, B. Güttler, M. Gospodinov, and L. Konstantinov, J. Phys. Condens. Matter **14**, 1091 (2002).

[30] H. Taniguchi, M. Itho, and D. Fu, J. Raman Spectrosc., **42**, 706 (2011).

[31] A.-M. Welsch, B. J. Maier, B. Mihailova, R. J. Angel, J. Zhao, C. Paulmann, J. M. Engel, M. Gospodinov, V. Marinova, and U. Bismayer, Z. Kristallogr. **226**, 126 (2011).

[32] A. Slodczyk, P. Daniel, and A. Kania, Phys. Rev. B **77**, 184114 (2008).

[33] M. I. Aroyo, A. Kirov, C. Capillas, J. M. Perez-Mato, and H. Wondratschek, Acta Crystallogr. Sect. A **62**, 115 (2006).

[34] B. Maier, B. Mihailova, C. Paulmann, J. Ihringer, M. Gospodinov, R. Stosch, B. Güttler, and U. Bismayer, Phys. Rev. B **79**, 224108 (2009).

[35] O. Svitelskiy and J. Toulouse, Phys. Rev. B **68**, 104107 (2003).

[36] B. P. Burton, E. Cockayne, S. Tinte, and U. V. Waghmare, Phase Transitions **79**, 91 (2006).

[37] R. H. Chen, C. T. Chang, and T. M. Chen, J. Phys. Chem. Solids **57**, 25 (1996).

[38] E. Salje, V. Devarajan, U. Bismayer, and D. M. C. Guimaraes, J. Phys. C: Solid State Phys. **16**, 5233 (1983).

[39] E. Husson, Key Eng. Mater. **155/156**, 1 (1998).

[40] A. I. Frenkel, D. M. Pease, J. Giniewicz, E. A. Stern, D. L. Brewe, M. Daniel, and J. Budnick, Phys. Rev. B **70**, 014106 (2004).

[41] R. E. Cohen, Nature **358**, 136 (1992).

[42] P. G. D. Clem, D. A. Payne, and W. L. Warren, J. Appl. Phys. **77**, 5865 (1995).

[43] M. Kumaresavanji, L. L. L. Sousa, F. L. A. Machado, C. Adriano, P. G. Pagliuso, E. M. B. Saitovitch, and M. B. Fontes, J. Phys. Condens. Matter **22**, 236003 (2010).

[44] M. Itoh, M. Shikano, and T. Shimura, Phys. Rev B **51**, 16431 (1995).

[45] Z. Ropka, R. J. Radwanski, and A. J. Baran, Physica C **387**, 262 (2003).

[46] I. W. Chen, J. Phys. Chem. Solids **61**, 197 (2000).

[47] B. Mihailova, R. J. Angel, A.-M. Welsch, J. Zhao, J. M. Engel, C. Paulmann, M. Gospodinov, H. Ahsbahs, R. Stosch, B. Güttler, and U. Bismayer, Phys. Rev. Lett. **101**, 017602 (2008).

[48] B. J. Maier, R. J. Angel, W. G. Marshall, B. Mihailova, C. Paulmann, J. M. Engel, M. Gospodinov, A.-M. Welsch, D. Petrova, and U. Bismayer, Acta Crystallogr. Sect. B **66**, 280 (2010).

[49] E. Dul'kin, B. Mihailova, G. Catalan, M. Gospodinov, and M. Roth, Phys. Rev. B **82**, 180101(R) (2010).

[50] K. Z. Baba-Kishi and M. Paściak, J. Appl. Crystallogr. **43**, 140 (2010).

[51] N. Takesue, Y. Fujii, M. Ichihara, and H. Chen, Phys. Rev. Lett. **82**, 3709 (1999).

[52] E. Dul'kin, E. Mojaev, M. Roth, I. P. Raevski, and S. A. Prosandeev, Appl. Phys. Lett. **94**, 252904 (2009).